Digitization of optical lever instruments

Giovanni Romeo
Istituto Nazionale di Geofisica, Roma, Italy

Abstract
Some classical old-fashioned instruments (such as the Wood-Anderson seismometers), as well as some modern instruments (like the all-quartz made Verbaandert-Melchior tiltmeters), conventionally require an impractical recording system obtained by a photographic drum recorder in a darkroom. Simple electronic equipment (made by readily available, low cost electronics) may help in using such kind of instruments allowing a useful digital recording. This will reduce the time-hour in data acquisition and storage (and the manual error), and will increase the accuracy. The theory of operations and some results obtained using the described equipment are shown.

Key words *optical lever – digitization – DSP – CCD linear sensor – Wood-Anderson – Grotta Gigante pendulums*

1. Theory of operation

The described system assumes a mechanical instrument which outputs the angle to digitize. The instrument's history is full of devices of such kind. Most of them are obsolete (there were mirror galvanometers exhibiting surprising sensitivities, characteristic of modern expensive digital instruments), but some of them still resist because of their historical importance, like the Wood Anderson seismometer (Richter, 1935), originally used for estimating earthquake magnitude. Some of them are unique instruments, like the 100 m long Grotta Gigante Pendulums (Marussi, 1960; Braitenberg, 1999). Others are still used, like the all-quartz made (Verbaandert-Melchior) (Agnew, 1986) tiltmeters because they provide an excellent measurement quality.

The principle is quite simple. A light beam hits a mirror tied to the moving part of the instrument, the reflected beam reaches an electronic sensor. The sensor measures the displacement of the light spot, which, for small angles (long optical arm, *i.e.* large amplifications) coincides with the angle under measurement.

Figure 1a,b illustrates the block diagrams of the angle meter. The target of the optical lever consists of a CCD linear array. A CCD optical sensor (charge coupled device, see Appendix A3) is an array of photosensors embedding an interface to allow a sequential transmission of the array content. The array length (proportional to the physical length of the sensor) represents the laser target dimension, and the length of the optical lever must be tuned to allow the whole system to stay in range. The measurement of the laser spot position is performed by a DSP connected to the CCD by a flash A/D converter.

The resolution of the CCD (1/number of pixels) is increased by one order of magnitude

Mailing address: Dr. Giovanni Romeo, Istituto Nazionale di Geofisica, Via di Vigna Murata 605, 00143 Roma, Italy; e-mail: romeo@ingrm.it

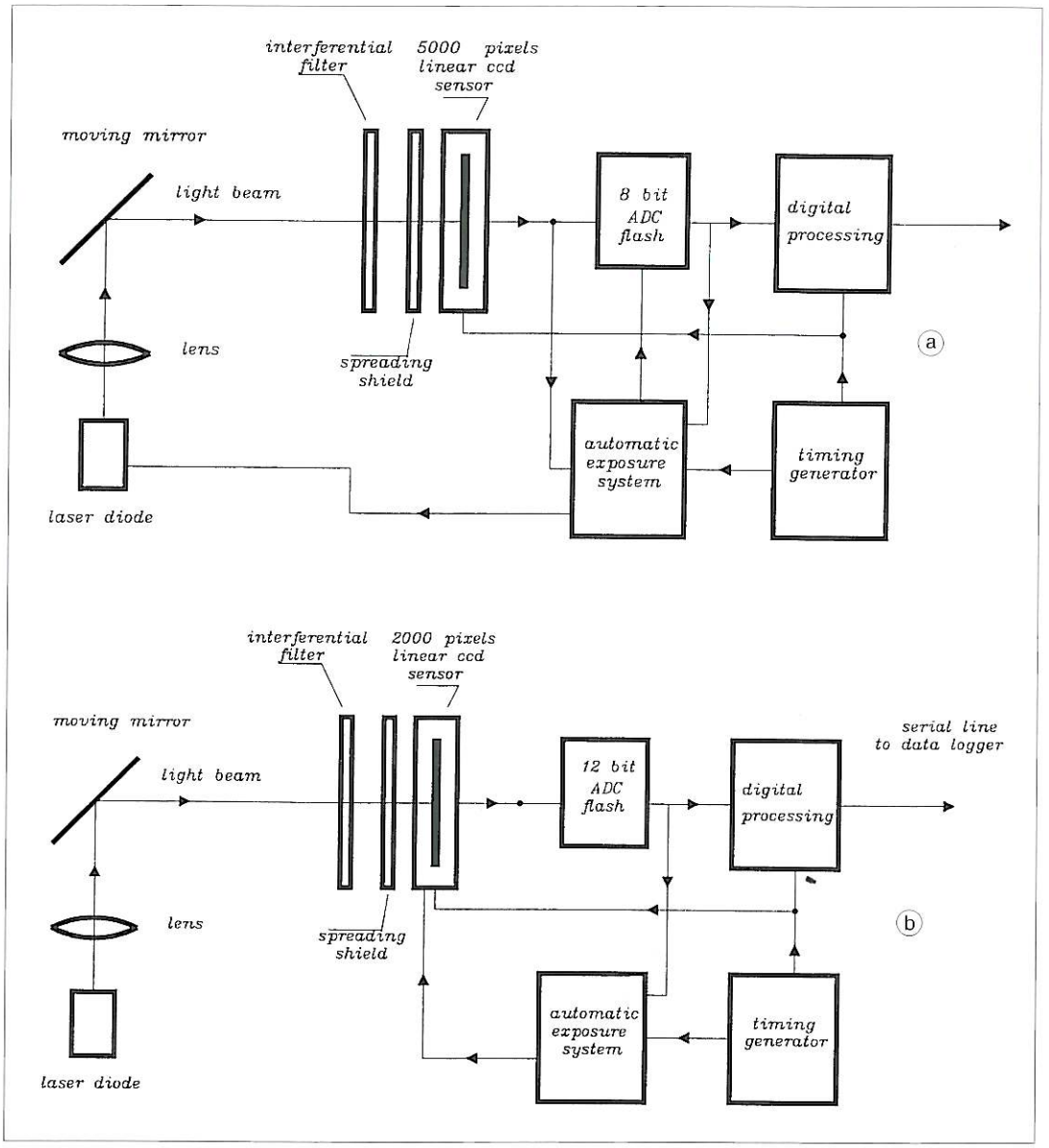

Fig. 1a,b. Theory of operation of the optical angle meter. The system uses a visible laser diode with its own lens. This is the only lens the system requires. An interferential optical filter (5 nm bandwidth) neglects the environmental light, and lets the system work in an ordinary lit room. The spreading shield before the CCD smoothes the light distribution shape on the sensor. This transforms the box-like light distribution shape over the sensor to a symmetrical Gaussian-like form. In this way the processor obtains more information to detect the center of the distribution. The two prototypes block diagram are very similar. Fundamental blocks are the same, but they act in different ways. a) Shows the first (simpler) one; b) shows the second one (faster and more sophisticated).

using real time data processing which evaluates the center of the light spot using the information available over the entire array.

Using a laser instead of an ordinary bulb helps avoid the focusing task necessary for non collimated sources; the system does not require any lens, except the one embedded in the laser source. The solid state laser allows an easy control of the beam intensity; it is very common to have solid state laser sources with a built-in photo-diode for continuous measurement of the laser intensity. A feed-back circuit may use the photo diode and an external control signal to modify the laser output.

An interferential filter (5 nm bandwidth) provided at the optical input allows the system to work in an illuminated environment.

Two prototypes were built using the same basic idea.

– The first (less performing) one used a 5000 pixels CCD, an 8 bit A/D converter and a single DSP chip (with minimum external hardware) to calculate the center of the light distribution. The resolution obtained was 1/40000 at 25 sps; this means that the system behaved like a 15 bit a/d converter which outputs 0 when the laser spot is in the left extremity of the sensor and 40000 when the spot is on the other side. It used a mixed analog and digital exposition system (Romeo, 1996) to constrain the A/D converter to stay in range, and controlled (for the same purpose) the intensity of the light beam.

– The second one employed a 2000 pixel CCD with the electronic shutter, a 12 bit A/D converter, some dedicate computing hardware, and a DSP chip to refine the calculation and filter the digitized signal. The resolution was approximately the same as the first one, but with the sample rate increased to 2000 sps. It used the CCD shutter to obtain a fully digital exposition system (Romeo and Rao, 1998), without the need to control the laser power.

2. Spot position detection

One objective of the position detector is to increase the precision on the spot position with regard to the CCD spatial resolution. The spatial intensity distribution of the laser spot is almost constant near the center and drops quickly at the boundary. When the laser hits against the monodimensional CCD array it will appear similar to a box-like function with smooth extremities.

In fig. 2 the solid line represents the CCD array content when the beam points directly on

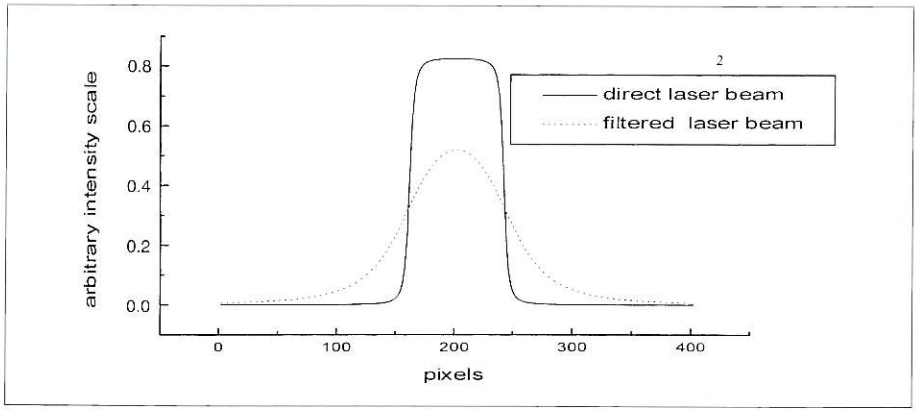

Fig. 2. The laser light distribution is very similar to a smooth box function. In the picture we assumed a 100 pixel wide spot striking on the 200th pixel against a 400 pixels the array (continuous line). After introducing a spreading shield near the CCD sensor, the light distribution becomes quasi-Gaussian (dotted line). This increases the center detection algorithm precision.

the sensitive area. In the picture it was assumed to have a 100 pixel beam centered at the 200th pixel. In the worst case of a vertical edged shape the error in detecting the center of distribution cannot be smaller than half pixel; in fact, in this case the information comes only from the edges of the distribution, which affects only few (at least one) pixel per edge. To increase the precision it is necessary to obtain more information about the pixel level. This is done by introducing a spreading shield near the sensor. This modifies the distribution to a Gaussian-like shape fig. 2, dotted line plot (see Appendix A1).

In this case we may calculate the optical central point using the formula

$$\rho = \frac{\sum_k k \cdot I(k)}{\sum_k I(k)}$$

where p is the center of the light spot, k is the position of the kth pixel and $I(k)$ is the light intensity on the kth pixel.

The error introduced using this strategy (sampling the pixel level with an 8 bit ADC) is one order of magnitude smaller than the one just based on the most lit pixel position (see Appendix A2). Unfortunately this method is sensitive to background light. A constant environmental light may increase the background level in the distribution, bringing the computed position to the center of the sensor. This effect can be avoided by tuning the automatic exposure system to bring the distribution's tails to 0. This is very efficient neutralizing a uniform environmental light. The prototype uses a dark glass spreading shield which allows the system to naturally neglect the disturbing light, which is weak compared with the laser beam, and helps the CCD to stay in range when lit by the laser beam. The interferential filter placed at the system optical input allows it to be practically insensitive to the environmental light.

3. Electronics

The optical sensor is based on a low cost CCD array (the first one used a SONY ILX501, the second one an ILX703A) (Sony, 1992) made for FAX machines, both of them can be very easily interfaced. The A/D converters used were by Thomson and Burr-Brown, low cost, made for video purposes. The first prototype (used with the ILX501) provides the control of the comparators reference resistors array in order to operate the automatic exposure system. The second one had a higher speed and it was used with the ILX703A; in this case the exposure system was performed using the CCD shutter facility, and did not require A/D control. It is not necessary to have a high quality A/D (in terms of integral linearity), because the A/D linearity modifies only the distribution's shape, but does not affect its symmetry and, therefore, the position of the center of the distribution.

The computing system was based on a DSP and MAC (Multiply and Accumulate) chips (fig. 3). We used Motorola and TI DSP; both of them offer enough internal resources to operate with a very small amount of external hardware. MAC chips were from TRW. All glue logic was implemented in EPLD (Erasable Programmable Logic Device). The first prototype used just the Motorola DSP, some analog circuitry, and its capability was of 25 sps, with a resolution of 1/40000. The second prototype had roughly the same resolution, but its capability was of 2000 sps because of the MAC speed. The second prototype included a digital filter and decimation program useful for seismological purposes. The use of a low pass digital filter offers an even better resolution because the filter operates a weighted average of several samples. Both prototypes interfaced the external world by a 9600 baud asynchronous serial line. Figure 3 shows how two MAC chips were used to calculate part of the center of the light distribution.

4. Test and results

Both light position digitizer prototypes were tested in the lab, to evaluate their characteristics. The first one has been used in the field digitizing a Wood Anderson seismometer and the Grotta Gigante pendulums. A rugged version of the first one was used to digitize the sun position in the Boomerang balloon (Lange *et al.*, 1995) orientation system.

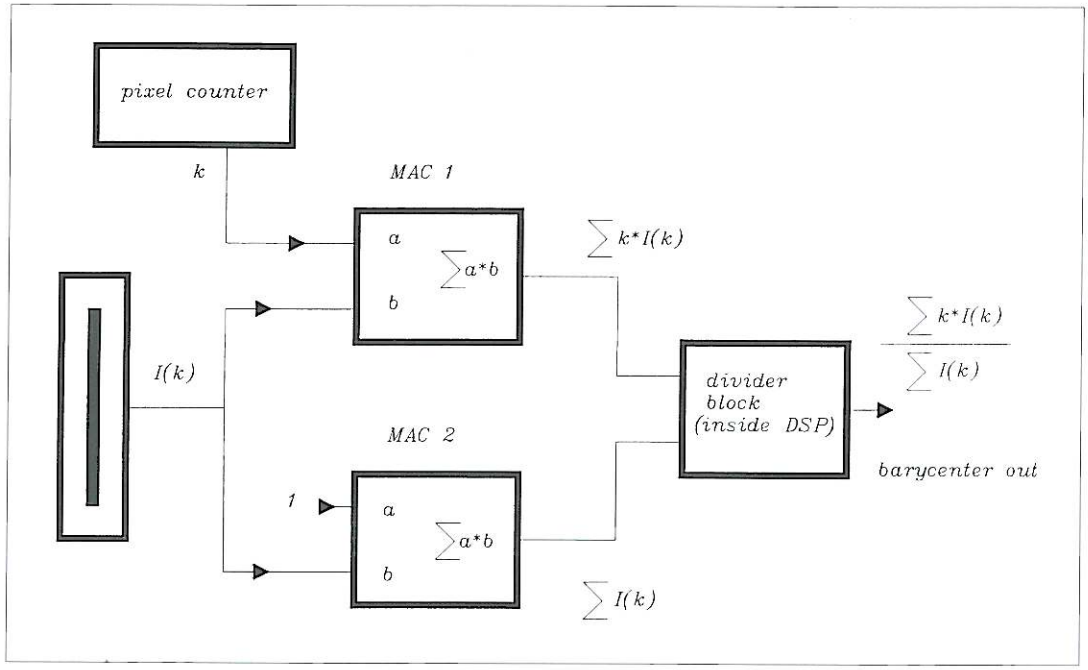

Fig. 3. The use of MACs to calculate the barycenter. MACs are dedicated chips that can perform Multiply and ACcumulation task. MAC 1 input is connected to a pixel counter input and to the CCD A/D converter, and produces the barycenter formula numerator. MAC 2 just accumulates the A/D converter output, and produces the barycenter formula denominator. The two partial results are divided inside the DSP. With 2000 sps this circuits performs 4 000 000 multiplications per second (plus 4 000 000 sums and 2000 divisions). The use of MACs saves a lot of DSP time so it may perform some other task like filtering and decimation.

The lab test was conducted using a rotating, computer-controlled platform, holding the system and a focusing system (a stenopeic passage for the light). Rotating the platform we moved the image of the bulb focused on the CCD plane over the entire array (fig. 4).

Figure 5a-c shows some results from the test apparatus. In fig. 5a we report the light position measured on a range of ± 60° of platform rotation. The test was conducted by moving the platform by 1° steps, and recording 100 times the output angle. Figure 5b,c show the 100 values recorded for an angle close to 0° and the 100 values recorded for an angle close to 60°. The peak-to-peak amplitude of fig. 5b,c may be considered as the system maximum error. The ratio between the error counts and the whole range counts gives the precision of the system. In the worst case it is about 1/40 000, a bit better than a 15 bit A/D. The system performs even better; in fact the error at the CCD extremities increases because of the experimental assembly: the image of the bulb focused on the array is spread and distorted by the large incidence angle.

Although the second sensor has been built using a smaller CCD, a more resolute A/D allowed the system to reach the same characteristic, but with a sample rate 100 times faster.

Only the simpler prototype had a field test until now.

The first field application of the digitizing system was built around a Wood Anderson seismometer (made by Teledyne-Geotech). The sys-

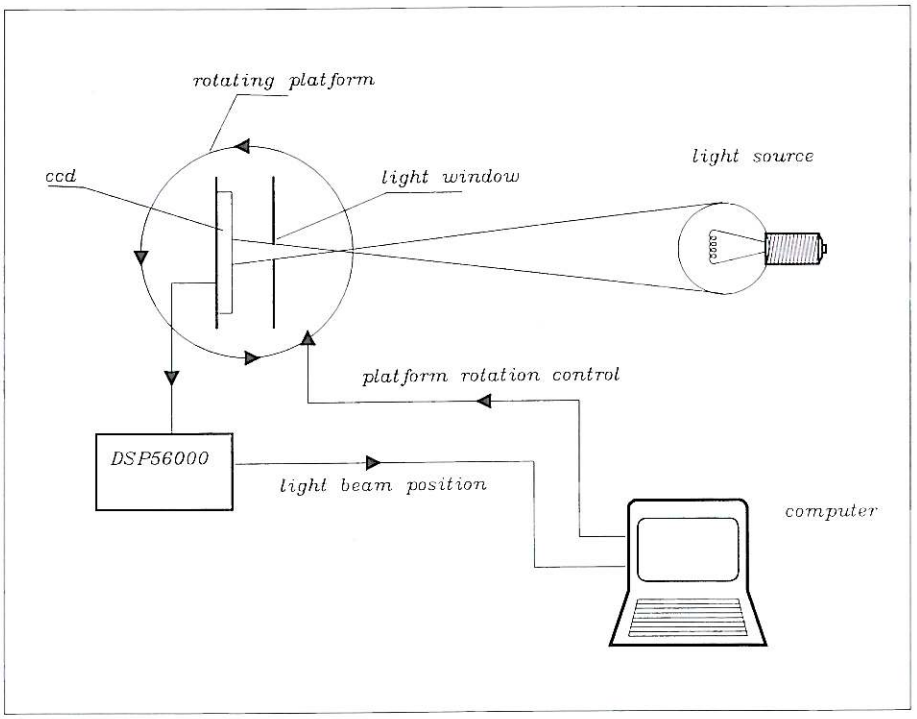

Fig. 4. Test apparatus for the digitizing system; the computer controls the rotating platform position, and receives data from the DSP processor. The center of the light distribution over the sensor is proportional to the tangent of the platform angle.

tem was installed in the Monteporzio Observatory during summer 1995, and was active during the seismical sequence (14 events in two days) starting on 12th June. The natural logarithm of the displacement was compared with the magnitude computed by a local seismic network operating around the epicentral area (Amato *et al.*, 1994). All the events had a common epicenter and there was no need for a distance correction. Figure 6 shows the comparison between the Wood Anderson maximum displacement, and the magnitude.

Although good for the magnitude estimation, the 25 sps digitizer is not enough for a good quality recording, because of the weak sample rate. The WA outputs frequencies that exceed 12.5 Hz, and we may not put an anti-aliasing filter on a light beam!

The same consideration on the aliasing introduced by the system and related problems are shown in Appendix A3.

The system was also used to digitize the Grotta Gigante pendulums (Marussi, 1960). They are horizontal pendulums with Zöllner type suspension (fig. 7). Here both upper and lower mountings are fixed to the solid rock of the cave itself, ensuring great stability for the attachments of the wires supporting the pendulums. Furthermore, this causes a different response to local deformation, from the ordinary tiltmeters. The peculiar characteristic regards the natural period of the pendulums, related to the exceptional height of the cave (112-m height), allowed to attain a long natural period of the instruments (6 min). The pendulums are set at critical damping by oil bath dampers. A mirror

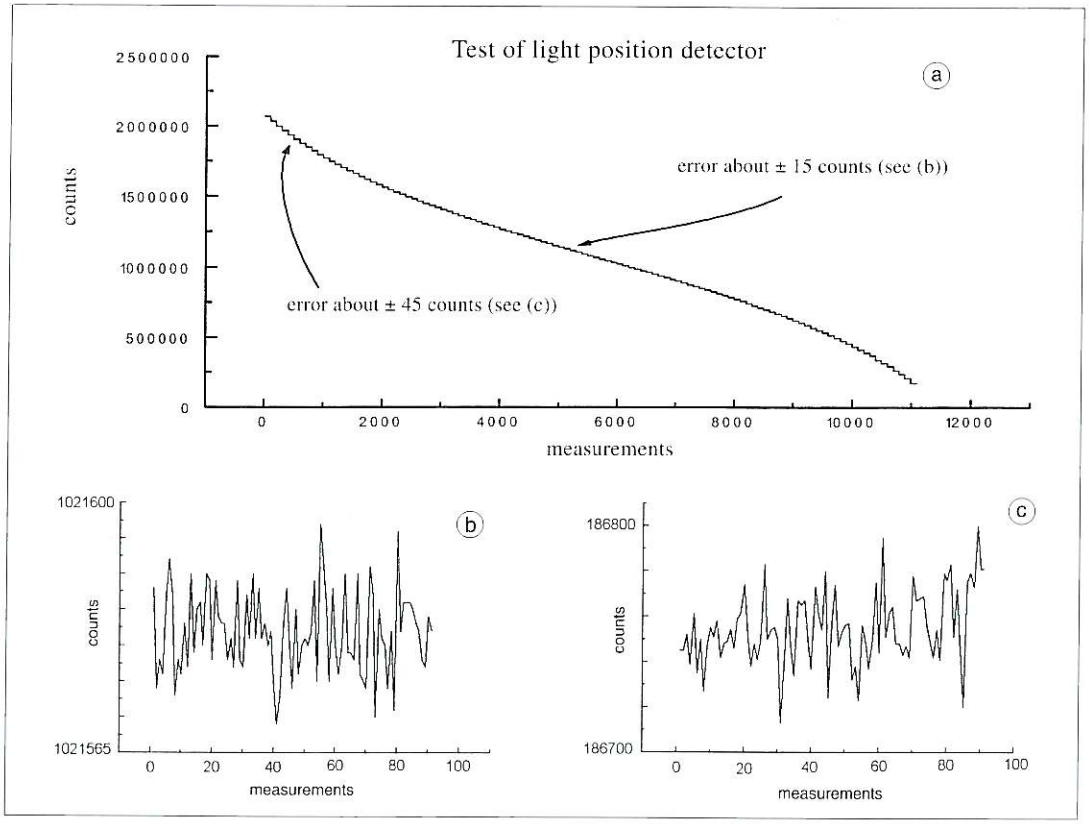

Fig. 5a-c. a) Represents the measurement for 120° platform rotation (fig. 4). The platform is rotated by 1° step, and 100 samples were acquired for each step. Two steps (indicated in (a)) were zoomed in (b) and (c). Note the vertical scale difference between (b) and (c).

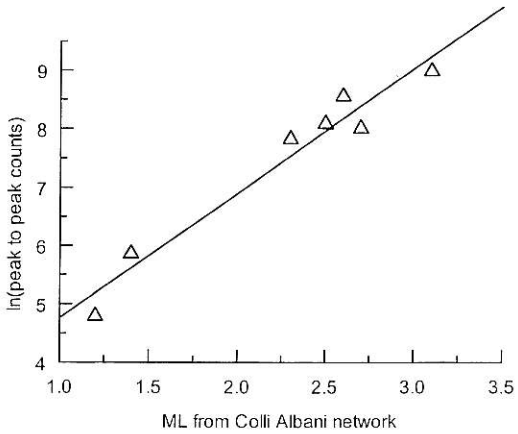

fixed to the rotation axis of the boom allows the use of an optical lever to detect the pendulum oscillation. The essential mechanical characteristics of the pendulums (values for NS component) are reported in table I.

Fig. 6. Comparison between the WA displacement and the magnitude computed from the Colli Albani network. We used just the log of the displacement because all the events had the same epicenter.

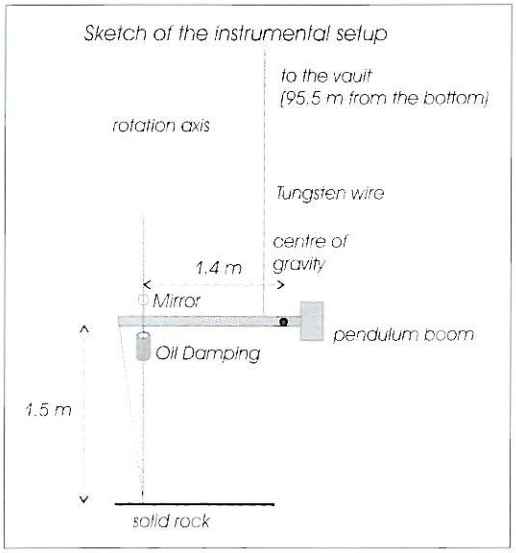

Fig. 7. The Grotta Gigante pendulums assembly (after Marussi, 1960; Braitenberg, 1999).

Table I. Grotta Gigante pendulums characteristics.

Distance between upper and lower mountings	95.5 m
Total weight of the pendulum, including wires	18.340 kg
Distance of the center of gravity from the rear suspension	141.7 cm
Period of oscillation in the horizontal plane	360 s
Damping	critical

The digitizing system has been operated for several months in the Grotta Gigante, and allowed the seismological use of the pendulums. As an example fig. 8 shows a seismic event, recorded by the digitized pendulum, compared with the vbb station installed in the same site.

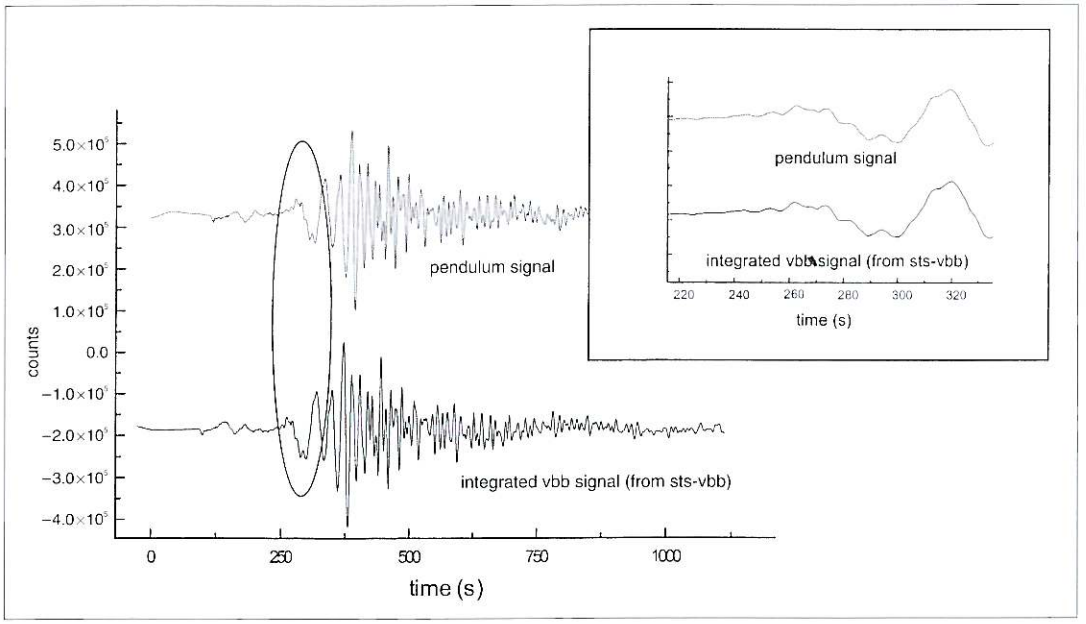

Fig. 8. The event of 20th July 1996 (GMT 00:00) in Turkey recorded by the N-S pendulum and the E-W component of the OGS vbb station in the Grotta Gigante. To make the two traces display the same physical quantity, the signal from the vbb was integrated. The circled zone is zoomed in the picture superimposed to disclose the two signals' likeness.

5. Conclusions

In this paper we described the use of CCD linear sensors to digitize the position of a laser spot. The use of dedicated electronics and optics helped us to obtain more than 15 bit precision at 2000 samples per second, working in a lit environment. Some experimental results have been shown to demonstrate the use of the system for geophysical purposes. Unlike analog position detectors a CCD-based system offers a time stability that is tied only to the mechanical assembly quality, and so may be used for seismological purpose as well as for tiltmetric purposes.

Acknowledgements

Several persons helped the author to build and test the prototypes.

Francesco Pongetti designed the printed circuit board for the first prototype and helped installing and testing it. Carla Braitenberg operated the installation on the Grotta Gigante pendulums and treated the collected data. Valerio Visentini extensively tested the first prototype, and Sandro Rao built the second one as part of his degree thesis. The simulations shown in the paper are from his thesis.

Appendix

A1 *Effect of the spreading shield*

A «first order» spreading shield effect may be computed considering 0 thickness spreading layer and a box-distributed laser beam. Every point of the laser spot on the shield surface can be considered an individual spherical light source. A target lit by this receives a light distribution

$$I(x,d) = A \cdot d \cdot (d^2 + x^2)^{-\frac{3}{2}} \qquad (1)$$

where A indicates the source intensity, d the distance between the shield and the target and x the coordinate on the target (fig. 9). To know the distribution shape produced by the entire spot we may integrate the previous formula over the entire spot surface. The calculus is simplified because we need the response only over the sensor array. The laser spot shape is included in the dependence of the intensity, A, by the spot coordinate, X

$$I(x) = \int_{\text{spot}} A(X) \cdot d \cdot (d^2 + (x - X)^2)^{-\frac{3}{2}} dx \qquad (2)$$

where $A(X)$ in the case of a round spot of radius r is

$$A(X) = \frac{1}{2}(r\sqrt{r^2 + d^2} + d^2(\ln(r + \sqrt{r^2 + d^2}) - \ln(d)))$$

$$\text{for } |X| \le r, \quad 0 \text{ elsewhere.}$$

By integrating the (2) we obtain smooth distribution shapes.

Figure 10 evidences the shapes of light distribution, moving the distance between the spreading shield and the CCD sensor. The best distribution has a smooth shape and tails which do not reach the end of CCD (this avoids errors in the center calculation). This may be obtained by moving the ADC range to give the LSB a value greater than 0. This will cut away the distribution tails, increasing the system dynamic range (fig. 10). The best results are obtained when the distance shield-CCD has the same order of magnitude as the spot diameter. The calculus just shown is an approximation of the real world, where we do not have 0 thickness spreading shields, or box-shaped light beam, but the measurements performed on the prototype confirm the approximation is good enough for practical purposes.

A2 *Precision in center detection*

The center detection is performed using the «center of mass» formula

$$p = \frac{\sum_{k=1}^{N} k \cdot I(k)}{\sum_{k=1}^{N} I(k)} \qquad (3)$$

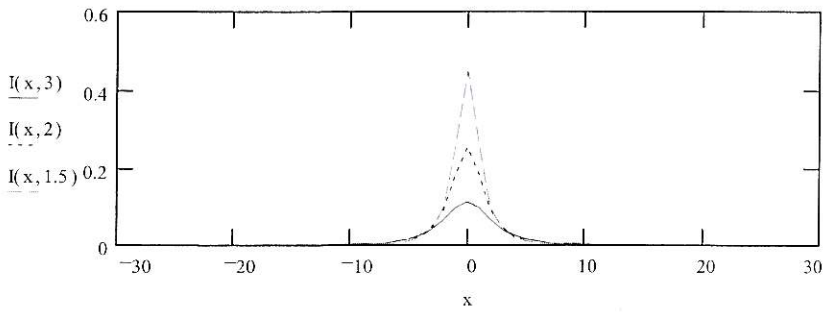

Fig. 9. The light distribution produced by a pinpoint source on a flat target.

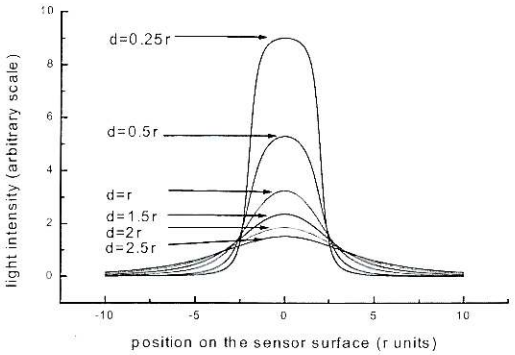

Fig. 10. Shapes of the light distribution as a function of the distance between the CCD sensor and the spreading shield.

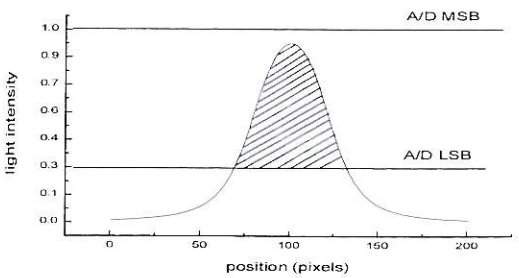

Fig. 11. The figure represents a light distribution of a spread laser beam on a 200 pixels target. The LSB of the A/D converter has been moved to 30% of the whole scale. In this case only the dashed zone is considered by the system. This avoids the tail of the distribution overcoming the CCD ends, and increases the dynamic range.

where $I(k)$ is the light intensity on the kth pixel, P is the center of the light distribution and N is the number of pixels.

We may neglect the error coming from the sensor geometry, and assume that the major part of the error is due to the sampling system

$$E_p^2 = \sum_{i=1}^{N} \left(\frac{\partial}{\partial I(i)} \frac{\sum_k k \cdot I(k)}{\sum_k I(k)} \right)^2 \cdot \Delta_i^2 . \qquad (4)$$

Equation (4) is obtained using the classic error propagation theory, and Δ_i represents the error introduced by the ith pixel.

The use of the (4) is impractical in the real case of the light distribution, and a numerical simulation has been used to evaluate the system error. Anyway the basic idea is that a N points light distribution gives $N/2$ measurement of the light barycenter. An average of $N/2$ measurements decreases the error by $1\sqrt{N/2}$.

The error will depend on:

– the number of the CCD pixels,
– the resolution of the A/D converter,
– the number of lit pixels (depending on the distance between the CCD and the spreading shield).

In the simulation we assumed a 2000 pixels CCD and we parameterized the a/d resolution and the number of lit pixels.

We assumed the sampling error as a random noise with a maximum value of ± ½ count.

The light distribution was a 2nd order curve (but any symmetrical light distribution works correctly) (5)

$$I(k) = \begin{cases} \alpha \cdot \sqrt{r^2 - (k - n \cdot l)^2} & ; \; n \cdot l - r \le k \le n \cdot l + r \\ 0 & ; \text{ otherwise} \end{cases} \tag{5}$$

where k (continuous value) represents the center of the distribution, r is proportional to the number of lit pixels, n (discrete value) is the pixel number and l represents the length of one pixel.

The simulation was conducted in this way.

After fixing the r k and the A/D resolution, the (3) was used to calculate the barycenter (with random error added to it to simulate the A/D resolution); the absolute value of the difference between the computed k and the predefined k gives an error Δ_{k1}.

This calculation was performed for several values of k (the distance between these values was less than one pixel) in order to make a good mean. This procedure has been repeated for several values of r. The result of this procedure is shown in fig. 12.

It is intuitive that the error decreases when the distribution becomes larger, because there are more points involved in the barycenter computation. The wideness of the light distribution must not be increased too much, because it does not overcome the CCD ends. In addition, as we increase the precision by enlarging the distribution we reduce the space where the distribution can move, therefore reducing the system's dynamic range. The desired result in this digitizer is to obtain the maximum number of significant counts between the extremity of the range; this can be written as a function of r

$$D(r) = \frac{2000 - 2 \cdot r}{err(r)}. \tag{6}$$

The plot of this function (fig. 13) shows a maximum at 400 pixels on a 2000 pixels CCD.

The dependence on the A/D resolution (expressed in counts) has been reported in fig. 14.

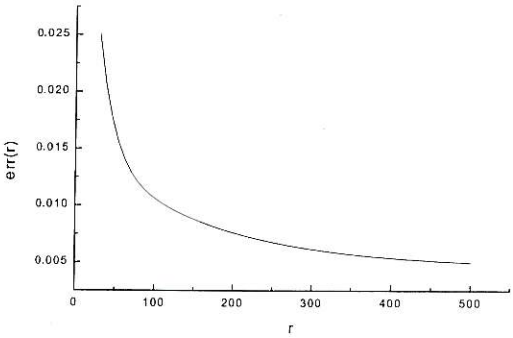

Fig. 12. The diagram shows the error made using a 2000 pixels CCD *versus* the radius of a circular light distribution shape expressed as number of pixels. The error decreases as the radius of the distribution increases, because more points are involved in the barycenter determination.

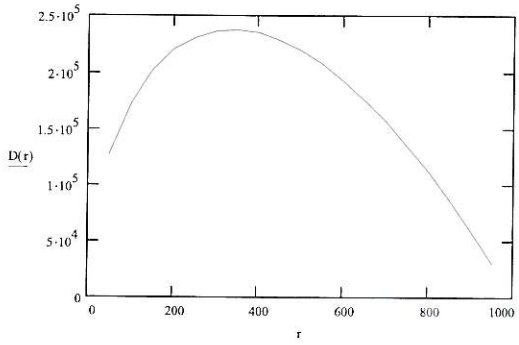

Fig. 13. Plot of the dynamic range of a 2000 pixels CCD *versus* the width of the light distribution expressed as number of pixels.

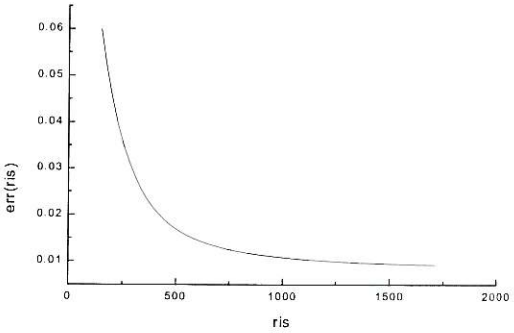

Fig. 14. The system error (pixels) *versus* the A/D resolution (counts). The dependence stops being significant when the A/D resolution is greater than 10 bits.

So the recipe for obtaining the best performance from the system is:

– Place the spreading shield at the right distance from the CCD (fig. 10) to tune the dome of the curve to have the right size (according with the 6 for the best dynamic range).

– Cut the distribution tails moving the A/D range to retail the distribution dome (fig. 11).

A3 *Aliasing consideration*

To better understand the way the signal is sampled and how the aliasing phenomenon may affect the system, it is useful to examine how the CCD sensor works.

A CCD sensor block diagram is shown in fig. 15.

The output of a single pixel (H) after the exposure time T is given by

$$H = \int_0^T l * L(t)dt \tag{7}$$

where l represents the efficiency of the conversion, and L the light intensity.

Once the T time has elapsed, the charge in the sensor is transferred to the analog shift register, and the sensor content is cleared. This transfer time is significantly shorter than the exposure time.

If a moving beam hits the CCD sensor surfaces, the intensity recorded by the sensor after the time T has a fancy shape shown in fig. 16, that illustrates the case of an exponentially decaying sine.

Figure 16 shows the intensity distribution diagram recorded in the CCD sensor generated by a moving light spot. Each point in the light distribution was computed using (3). It is easy to demonstrate that the barycenter of the light distribution coincides with the arithmetic mean of the signal in the time domain: the arithmetic mean of the signal in the time T is given by

$$\frac{1}{T}\int y(t)dt. \tag{8}$$

The level of the intensity distribution over the segment of the length dy is proportional to the stationing time of the light spot over dy, *i.e.*

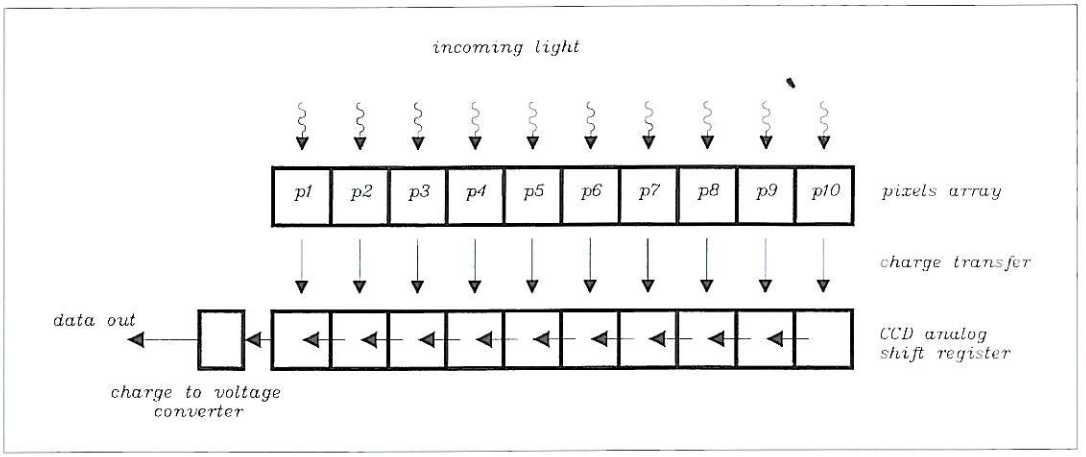

Fig. 15. A CCD optical array sensor. A series of light sensors (pixels: hole accumulation diodes, p1 ... p10) is the target of a light beam. The light generates a number of holes in the diode which depends of the light intensity and the exposure time. A charge transfer device moves the charges to a CCD analog shift register which allows the data to be squeezed to the external circuitry through a charge to voltage converter.

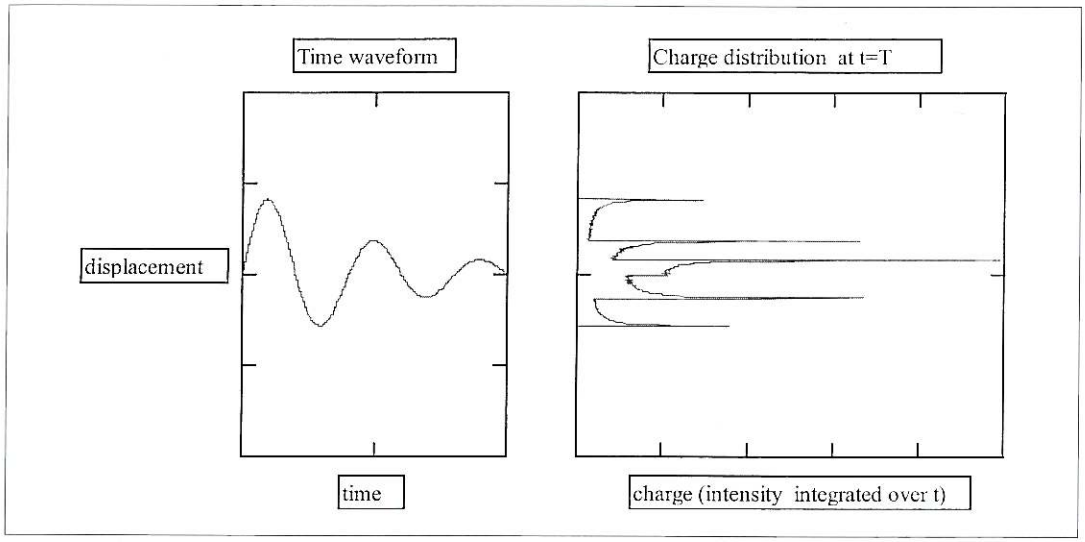

Fig. 16. Light distribution shape (right) generated by a waveform on the CCD sensor (left). The level of the light in a point distribution is proportional to the time the light spot stays on that point.

$\frac{dt}{dy}dy$. The barycenter position is given by

$$\frac{\int_0^y y\frac{dt(y)}{dy}dy}{\int_0^y dt(y)} \qquad (9)$$

after an exchange of variables (8) coincides with (9).

Each sample flowing through the system is a temporal average of the signal during the sample time T. This operates on the signal a low-pass and decimation process, producing an output data stream less aliased than a usually sampled signal.

A signal $y(t)$ sampled as just shown can be written as

$$y(n) = \frac{1}{\xi}\int_{nT}^{nT+\xi} y(t)dt \qquad (10)$$

where T represents the sampling period and ξ the integration time (it is, obviously, $T \geq \xi$). This coincides with the $y(t)$ when $T \to 0$ and $\xi \to 0$. When just $\xi \to 0$ the (10) represents an usually sampled sequence.

The frequency response of such type of sampling is shown in fig. 17, for different values of ξ.

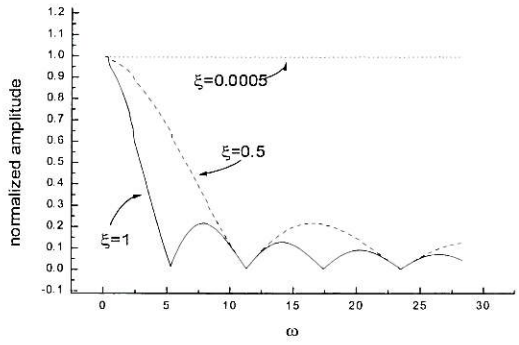

Fig. 17. The dot trace represents the frequency response of (10) in the case of $\xi \to 0$. The dash trace represents the case of ξ = ½ T. The solid trace is the case of $\xi = T$, as in the prototype. T = 1 for all traces.

We assumed $T = 1$ for all the traces in fig. 17. The Nyquist condition $\omega < \pi$ is not respected in any case if the spectrum of the incoming signal is flat.

However the system offers a better performance compared with a simple sampling system.

Although the results shown seem acceptable even for seismic purpose (in the shown cases the natural response of the instruments helped making a natural low-pass filter) the records are only apparently clean, and the slow prototype must apply only to the log of very slow systems, like tiltmeters.

The 2000 sps offered by the fast prototype are enough to produce an unaliased recording even of short period seismometer. This is because the high sample rate allows the instrument to record frequencies of 1 kHz. At this frequency the instrument attenuation has the same order of magnitude as the system resolution. So the signal is not aliased with a 2 kHz sample-rate. In addition, the built-in FIR filter and decimator of the second prototype offers an unaliased low frequency (*i.e.*, 25 Hz) sample rate.

REFERENCES

AMATO, A., C. CHIARABBA, M. COCCO, M. DI BONA and G. SELVAGGI (1994): The 1989-1990 seismic swarm in the Alban Hills volcanic area, Central Italy, *J. Volcanol. Geotherm. Res.*, **61**, 225-237.

AGNEW, D.C. (1986): Strainmeters and tiltmeters, *Rev. Geophys.*, **24** (3), 579-624.

BRAITENBERG, C. (1999): The Friuli (NE Italy) tilt/strain gauges and short term observations, *Ann. Geofis.*, **42** (4), 637-664.

LANGE, A., P. DE BERNARDIS, M. DE PETRIS, S. MASI, F. MELCHIORRI, E. AQUILINI, L. MARTINIS, F. SCARAMUZZI, B. MELCHIORRI, A. BOSCALERI, G. ROMEO, J. BOCK, Z. CHEN, M. DEVLIN, M. GERVASI, H. HRISTOF, P. MAUSKOPF, D. OSGWOOD, P. RICHARDS, P. ADE and M. GRIFFIN (1995): The boomerang experiment, *Space Sci. Rev.*, **74**, 145-150.

RICHTER, C.F. (1935): An instrumental earthquake magnitude scale, *Bull. Seismol. Soc. Am.*, **72**, 941-958.

MARUSSI, A. (1960): The University of Trieste station for the study of the tides of the vertical in the Grotta Gigante, in *Proceedings of the III International Symposium on Earth Tides, Trieste*, 45-52.

ROMEO, G. (1996): *Peak Detector Maximizes CCD-Sensor Range*, EDN, p. 88.

ROMEO, G. and S. RAO (1998): *Automatic-Exposure Scheme Uses CCD Shutter*, EDN.

SONY (1992): *Linear Sensor Application Note*, November.

(received November 25, 1999;
accepted April 4, 2000)